Chemical compositions of six metal-poor stars in the ultra-faint dwarf spheroidal galaxy Boötes I

M. N. Ishigaki[1], W. Aoki[2,3], N. Arimoto[2,3,4], and S. Okamoto[5]

[1] Kavli Institute for the Physics and Mathematics of the Universe (WPI), Todai Institute for Advanced Study, University of Tokyo, 5-1-5 Kashiwanoha, Kashiwa, Chiba 277-8583, Japan e-mail: `miho.ishigaki@ipmu.jp`
[2] National Astronomical Observatory of Japan, Mitaka, Tokyo 181-8588, Japan e-mail: `aoki.wako@nao.ac.jp`, `arimoto.n@nao.ac.jp`
[3] Department of Astronomical Science, The Graduate University of Advanced Studies, Mitaka, Tokyo 181-8588, Japan
[4] Subaru Telescope, National Astronomical Observatory of Japan, 650 North A'ohoku Place, Hilo, HI 96720, USA
[5] Kavli Institute for Astronomy and Astrophysics, Peking University, Beijing 100871, China e-mail: `okamoto@pku.edu.cn`

ABSTRACT

Context. Ultra-faint dwarf galaxies recently discovered around the Milky Way (MW) contain extremely metal-poor stars, and might represent the building blocks of low-metallicity components of the MW. Among them, the Boötes I dwarf spheroidal galaxy is of particular interest because of its exclusively old stellar population. Detailed chemical compositions of individual stars in this galaxy are a key to understanding formation and chemical evolution in the oldest galaxies in the Universe and their roles in building up the MW halo.

Aims. Previous studies of the chemical abundances of Boötes I show discrepancies in elemental abundances between different authors, and thus a consistent picture of its chemical enrichment history has not yet been established. In the present work, we independently determine chemical compositions of six red giant stars in Boötes I, some of which overlap with those analyzed in the previous studies. Based on the derived abundances, we re-examine trends and scatters in elemental abundances and make comparisons with MW field halo stars and other dwarf spheroidal galaxies in the MW.

Methods. High-resolution spectra of a sample of stars were obtained with the High Dispersion Spectrograph mounted on the Subaru Telescope. Abundances of 12 elements, including C, Na, α, Fe-peak, and neutron capture elements, were determined for the sample stars. The abundance results were compared to those in field MW halo stars previously obtained using an abundance analysis technique similar to the present study.

Results. We confirm the low metallicity of Boo-094 ([Fe/H]= −3.4). Except for this star, the abundance ratios ([X/Fe]) of elements lighter than zinc are generally homogeneous with small scatter around the mean values in the metallicities spanned by the other five stars (−2.7 <[Fe/H]< −1.8). Specifically, all of the sample stars with [Fe/H]> −2.7 show no significant enhancement of carbon. The [Mg/Fe] and [Ca/Fe] ratios are almost constant with a modest decreasing trend with increasing [Fe/H] and are slightly lower than the field halo stars. The [Sr/Fe] and [Sr/Ba] ratios also tend to be lower in the Boötes I stars than in the halo stars.

Conclusions. Our results of small scatter in the [X/Fe] ratios for elements lighter than zinc suggest that these abundances were homogeneous among the ejecta of prior generation(s) of stars in this galaxy. The lower mean [Mg/Fe] and [Ca/Fe] ratios relative to the field halo stars and the similarity in these abundance ratios with some of the more luminous dwarf spheroidal galaxies at metallicities [Fe/H]< −2 can be interpreted as star formation in Boötes I having lasted at least until Type Ia supernovae started to contribute to the chemical enrichment in this galaxy.

Key words. nuclear reactions, nucleosynthesis, abundances – galaxies: abundances – galaxies: dwarf – galaxies: individual(Boötes I) – stars: abundances

1. Introduction

Ultra-faint dwarf spheroidal galaxies (UFDs), recently discovered in the Local Group, provide us with an excellent laboratory for studying the formation of low-mass galaxies and production of heavy elements in their earliest stages in the Universe. The faint Boötes I dwarf spheroidal galaxy (dSph) is one of the most interesting objects of its kind as a candidate for first galaxies and/or as building blocks of the Milky Way (MW). It was first discovered with the help of photometric data obtained by the Sloan Digital Sky Survey (SDSS; York et al. 2000) as one of the faintest galaxies known to date (Belokurov et al. 2006). Subsequent spectroscopy to measure line-of-sight velocities of candidate member stars suggests that Boötes I is a dark-matter-dominated system with a total mass on the order of $10^7 M_\odot$ (Muñoz et al. 2006; Martin et al. 2007). Koposov et al. (2011)

has developed a reduction technique to derive more accurate radial velocities, and they suggest that the velocity dispersion of this system is represented better by two components with 2.4 km s^{-1} for a "cold" component and ∼ 9 km s^{-1} for a "hot" one, which could be interpreted as the result of velocity anisotropy in this galaxy.

Detailed analyses of a color-magnitude diagram (CMD) for Boötes I suggests that it consists of a very old stellar population with age > 10 Gyr, which is similar to the most metal-poor globular clusters in the MW (Okamoto et al. 2012). Chemical abundance analyses based on lower resolution spectroscopy report very low metallicities for Boötes I stars at [Fe/H]∼ −2.5 on average with a large spread of Δ[Fe/H]$\gtrsim$ 1.0 dex (Norris et al. 2008; Lai et al. 2011).

Detailed chemical abundances for Boötes I allow us to further address whether possible progenitors of the metal-poor component of the MW are similar to Boötes I and whether this galaxy is indeed an example of the first galaxies formed in the early Universe. However, these questions have not yet been clearly answered because of the discrepancy in abundance results among previous studies. Chemical abundances based on high-resolution spectroscopy for Boötes I stars have previously been obtained by Feltzing et al. (2009, hereafter F09), Norris et al. (2010b), and Gilmore et al. (2013, hereafter G13). Feltzing et al. (2009) analyzed seven stars with $-3 \lesssim$ [Fe/H] $\lesssim -2$ based on the high-resolution spectra using an LTE abundance analysis code that takes the sphericity of stellar atmospheres into account. They report the presence of a star with an anomalous [Mg/Ca] ratio, Boo-127, and interpret it as a signature of nucleosynthesis yields of individual supernove (SNe).

Gilmore et al. (2013) carried out the double-blind analysis by two groups of the co-authors, Norris & Yong (NY) and Geisler & Monaco (GM), for six stars in Boötes I with $-3.7 <$ [Fe/H] $<$ -1.9. They find that the chemical abundance pattern for the Boötes I stars are generally similar to those observed in field halo stars with small scatter. However, in contrast to what is generally known for the field halo stars with the similar metallicities, a signature of decreasing [α/Fe] ratios with increasing [Fe/H] is also suggested. They observed Boo-127 in common with F09 but did not confirm the [Mg/Ca] anomaly of this object. Although these data provide important implications for the early chemical enrichment of this galaxy, they provide the contrasting pictures, namely, the former study reports the presence of an anomalous star, which may suggest that the chemical evolution in Boötes I proceeded in an inhomogeneous manner, while the latter does not support the presence of this inhomogeneity.

To obtain a consistent picture of the early chemical evolution of Boötes I, we present an independent analysis of six Boötes I stars with $-3.2 <$ [Fe/H] < -2.0 based on high-resolution spectroscopic data obtained with the Subaru/High Dispersion Spectrograph (HDS). Five stars and three stars in our sample have been analyzed in common with F09 and G13, respectively.

This paper is organized as follows. In Section 2, we describe our sample, the method of observation, and equivalent width (EW) measurements. Section 3 presents the method for the stellar parameter and abundance estimates for the sample stars. In Section 4 we report the results of our abundance analysis and their comparison with previous results in the literature. Section 5 first presents the abundance comparison of the present Boötes I sample with the field MW halo stars and with other dSphs. Then, possible implications of the chemical evolution of Boötes I are discussed. Finally, Section 6 concludes the paper.

2. Observation and measurements

2.1. Sample and observation

The sample of six bright red giant branch stars in Boötes I was selected from Norris et al. (2008) to cover a wide metallicity range ($-3 \lesssim$ [Fe/H] $\lesssim -2$). The high-resolution spectra of six bright red giants were obtained with the Subaru Telescope High Dispersion Spectrograph (HDS; Noguchi et al. 2002) on 16-17 May 2009 and 16 May 2010. The objects are listed in Table 1 with observation details. We applied CCD on-chip binning (2×2 pixels), resulting in a resolving power of $R = \lambda/\delta\lambda = 40,000$. Our spectral ranges cover 4030–6800 Å. Spectra of two comparison stars in the Galactic halo (HD 216143 and HD 85773) were

Table 2. The Mg linelists.

λ (Å)	χ (eV)	F09[a]	G13(NY)[a]	G13(GM)[a]	TW[a]
			$\log gf$ (dex)		
4571.10	0.00	...	...	...	−5.623
4702.99	4.35	−0.666	...	...	−0.440
4730.03	4.35	...	...	...	−2.347
5172.68	2.71	−0.402	...	...	...
5183.60	2.72	−0.180	...	...	...
5528.40	4.35	−0.620	−0.340	−0.620	−0.498
5711.09	4.35	...	...	−1.833	...

Notes. [a] The $\log gf$ values for the Mg lines adopted in F09, G13, and this work (TW). The two independent analyses carried out by G13 are referred to as "NY" and "GM", respectively (see Section 1).

obtained with similar setups of the instrument in our previous run (Aoki et al. 2009).

A standard data reduction was made with IRAF echelle package. Cosmic-ray hits were removed by the method described in Aoki et al. (2005). The observations were carried out mostly during dark nights, and the sky background was not significant. One exposure of Boo–121 on 16 May 2010 was exceptionally affected by the Moon. We thus subtracted the sky background estimated from the slit image around the object. The spectra obtained from individual exposures were combined to obtain final spectra.

Radial velocities of the sample stars are measured from 25-50 Fe I lines for each object. The results are given in Table 1 ($v_{\rm helio}$). The measured values agree with those derived by G13 within 1.5 km s^{-1} for the three stars observed in common.

2.2. Equivalent width measurement

The EWs of absorption lines were measured by Gaussian fitting. The atomic line list used in Ishigaki et al. (2012, 2013) was adopted. The errors in the EW measurements estimated from the formula presented in Cayrel (1988) range from $\sim$ 5 to 12 m Å, depending on the signal-to-noise ratios ($\sim$ 10 per pixel at $\sim$ 4500 Å and $\sim$ 30 at $\sim$ 6000 Å) of the continuum.

Although Mg is a key element in our work, the gf values could be uncertain because of the lack of laboratory measurements for most of the Mg I lines (Aldenius et al. 2007). We inspected the gf values of Mg I lines adopted in previous studies for Boötes I stars F09 and G13 and summarize them in Table 2 (the values of F09 was provided by Feltzing, private communication). The last column gives the $\log gf$ values adopted in this work. The Mg I lines at 5172.68, 5183.60, and 5711.09 Å were not used in this work because EWs of these lines for our sample stars were too strong or too weak to be useful in the abundance analysis. As can be seen from Table 2, the $\log gf$ values for the 5528.40 Å line, which were common to all of these studies, are different by up to $\sim$ 0.3 dex.

We confirmed that the Mg abundances derived from different lines using the $\log gf$ values adopted in this work (last column of Table 2) agree within ~0.3 dex for the comparison stars, HD 216143 and HD 85773, for each.

2.3. Equivalent width comparisons

Figure 1 presents the comparison between the EWs measured in this work and those in G13 for the three stars analyzed in com-

Table 1. Objects and observations

Name	RA(J2000)	DEC(J2000)	g	$(g-r)_0$	$v_{\rm helio}$ (km s^{-1})	HJD
Boo–094	14:00:31.50	14:34:03.6	17.50	0.87	95.0±0.7	2454968
Boo–121	14:00:36.52	14:39:27.3	17.92	0.82	105.4±0.6	2454968
Boo–911	14:00:01.07	14:36:51.5	17.97	0.80	102.2±0.6	2454969
Boo–127	14:00:14.56	14:35:52.7	18.16	0.77	98.5±0.5	2455333
Boo–009	13:59:48.81	14:19:42.9	17.93	0.81	97.1±0.4	2455333
Boo–117	14:00:10.49	14:31:45.5	18.20	0.74	98.0±0.6	2455333

mon. For all of these stars, the EWs measured in this work are systematically lower than the values obtained by G13. The mean differences between the EW in this work and in the analysis of "NY" in G13 are 16-26 mÅ, while those between in this work and in the other independent analysis, "GM", in G13 are 10-18 mÅ, which are modestly larger than the errors in the EWs measurement (∼ 12 mÅ).

To test whether the uncertainty in the continuum placement could be the reason for the discrepancy, we examined the change in the measured EWs by adopting different continuum levels for one of the Fe I line as shown in Figure 2. For this line, the discrepancy in the measured EWs among the three analyses is particularly large (72.0 mÅ, 96.2 mÅ and 102.5 mÅ in this work, GM, and NY, respectively). If the continuum level of the normalized spectrum is changed by ±0.05, which is slightly more than the scatter in the continuum around this line (widths in the shaded regions), the measured EW varies in the range $52.7 - 89.2$ mÅ. This result illustrates that the variation in the continuum level partly explains the EW difference among the three analyses. However, as can be seen in Figure 2, the error in the continuum level that is as large as ±0.05 is unlikely for this line, so it is difficult to completely illuminate the discrepancy. In this paper, we use the measured EWs without any correction. Instead, we examine the effects of this offset in derived abundances in Section 3.3.

3. Abundance analysis

3.1. Stellar atmospheric parameters

Effective temperatures ($T_{\rm eff}$) were estimated based on *griz* color indices using the temperature scale of Castelli[1]. The *griz* photometry was adopted from the SDSS DR9 data set. The Galactic extinction in the *griz* magnitudes toward individual stars was corrected based on the revised extinction measurement by Schlafly & Finkbeiner (2011) via the NASA/IPAC Extragalactic Database[2]. The extinction in the *g*-band varies from 0.052 to 0.060 among our six sample stars. These values are translated into $E(B-V)$ in the Schlegel et al. (1998) from 0.016 to 0.018 (Schlafly & Finkbeiner 2011), which are consistent with the previously adopted value of $E(B-V)$= 0.02 (Norris et al. 2008).

The surface gravity (log *g*) for the sample stars are then estimated by comparing the adopted temperature with a 12 Gyr Yonsei-Yale (YY) isochrone (Demarque et al. 2004) by assuming that the stars lie on the red giant branch of the system. In the above procedure for obtaining $T_{\rm eff}$ and log *g*, the [Fe/H] values are needed as input. We adopt the initial guess of the [Fe/H] values from Norris et al. (2010a).

The microturbulent velocity (ξ) is estimated by requiring that the Fe abundances from individual Fe I lines do not depend on

---

[1] http://wwwuser.oat.ts.astro.it/castelli/colors/sloan.html
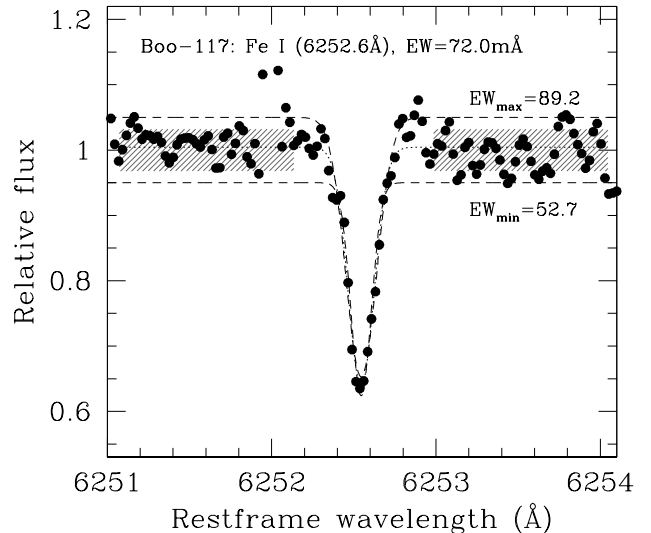[2] http://ned.ipac.caltech.edu/forms/calculator.html

Fig. 2. EW measurements for one of the Fe I lines by adopting the different continuum levels. The dotted line shows the best-fit Gaussian, where continuum level is estimated from the shaded wavelengths region. The dashed lines show the Gaussian fit by fixing the continuum levels to be ±0.05 of the best-fit value.

their measured EWs. In this step, we have used the Fe I lines having a reduced EW log(EW/λ) < −4.7.

After the standard 1D-LTE abundance analysis is performed, the procedures are iterated until a consistent set of parameters ($T_{\rm eff}$, log *g*, ξ, and [Fe/H]) is obtained. The resulting atmospheric parameters are summarized in Table 3.

The adopted $T_{\rm eff}$ and log *g* in this work and in the two independent analyses ("NY" and "GM") presented by G13 agree within 100 K and 0.2 dex, respectively, for the three stars analyzed in common. The ξ values are different between the two analyses in G13 by 0.5-1.3 km s^{-1}. The relatively high ξ value for Boo–094 reported by the "NY" analysis is in excellent agreement with ours, while the ξ values for Boo–117 and Boo–127 are more consistent with those obtained by the "GM" analysis.

3.2. Abundances

Abundances of individual elements are determined by standard analyses using the measured EWs. We restrict the analysis to the absorption lines with log(EW/λ) < −4.7 to minimize the errors in derived abundances. For Na I lines, we relax this restriction to log(EW/λ) ≤ −4.5, since only strong resonance lines are detected for this species. Similarly, only strong resonance Sr II lines are available for the abundance estimate of Sr. A spec-
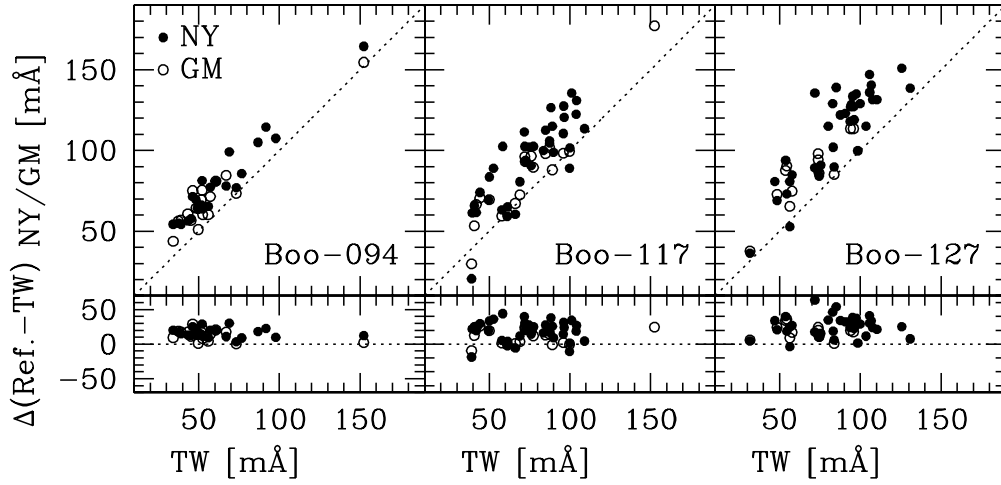
Fig. 1. Comparison of the measured equivalent widths (EWs) in this work (TW) and in the two analyses, "NY" (closed circles) and "GM" (open circles), in Gilmore et al. (2013).

Table 3. Atmospheric parameters

Object	$T_{\rm eff}$	$\log g$	ξ	[Fe/H]
	(K)	(dex)	(km s^{-1})	(dex)
Boo–094	4500	0.8	3.4	−3.2
Boo–121	4500	0.8	2.1	−2.5
Boo–911	4500	0.9	1.7	−2.2
Boo–127	4750	1.6	1.6	−1.9
Boo–009	4750	1.4	2.5	−2.7
Boo–117	4750	1.5	1.9	−2.2
HD216143	4529	1.3	1.9	−2.1
HD85773	4366	1.0	2.1	−2.4

tral synthesis is applied to estimate Sr abundances as described in detail in Section 4.7. The hyperfine splitting effect is included in the analysis of Ba lines (McWilliam 1998), assuming the r-process isotope ratios. The EWs and abundances estimated from individual lines are summarized in Table 4.

Carbon abundances are determined from the comparisons of synthetic spectra to the observed spectrum of the CH molecular band at around 4323 Å. For Boo–094, Boo–121, and Boo–009, only an upper limit of carbon abundance is estimated. Because the signal-to-noise ratios are low for the wavelength range of

the G-band, the continuum level is not determined well, which produces the abundance uncertainty of $0.1 - 0.3$ dex.

3.3. Abundance errors

The errors due to the line-to-line scatter ($\sigma_{\rm line}$), which are calculated as the standard deviation of the abundances from individual lines divided by the square root of the number of lines, are summarized in Table 5. If only one line is available for the abundance estimate, $\sigma_{\rm line}$ is assumed to be equal to the standard deviation for the Fe I lines, which are typically ~ 0.2 dex in the present work.

The abundance errors due to uncertainties in $T_{\rm eff}$, $\log g$, and ξ are examined by calculating the abundance differences when changing these parameters by ±100K, ±0.3 dex, and ±0.3 km s^{-1}, respectively. Results of this exercise are summarized in Table 5. The error bars in Figures 5 and 6, and $\sigma_{\rm tot}$ in Table 5 correspond to a quadratic sum of the contribution from the uncertainty in the three atmospheric parameters and line-to-line scatter in the abundances.

The systematic offset in the EWs from those in Gilmore et al. (2013) mentioned in Section 2.3 are an additional source of uncertainty in measuring absolute abundances in this work.
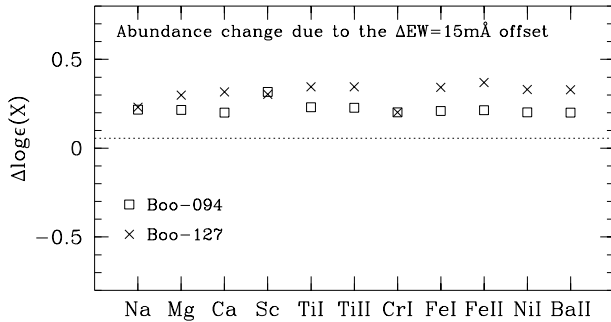
Fig. 3. Changes in abundances when all of the EWs in this work are increased by 15mÅ to partly correct for the EWs offset from Gilmore et al. (2013).

Figure 3 shows changes in $\log \epsilon(X)$ abundances when the EWs are increased by 15mÅ to reduce the systematic offset from the Gilmore et al. (2013) analyses for the most metal-poor (Boo–094) and metal-rich (Boo–127) stars in our sample. As can be seen, after the EW offset is applied, the abundances are systematically increased by $\sim 0.15 - 0.30$ dex. On the other hand, the amount of correction is mostly similar for all elements, and thus difference in the abundance ratios relative to iron ([X/Fe]) partly cancel out. Although the absolute abundances could be affected by the systematic errors in EW measurements, the abundance ratios ([X/Fe]) are consistent with those in Gilmore et al. (2013).

For the Sr abundances estimated by the spectral syntheses, uncertainty in the continuum level ($1\sigma \sim 0.1$) causes an error as large as ± 1.0 dex. as detailed in Section 4.7.

4. Abundance results

Our abundance results are summarized in Table 5. Relative abundances ([X/Fe]) were determined adopting the solar abundances from Asplund et al. (2009). Figures 5 and 6 plot the relative abundances of C, Na, Mg, Ca, Sc, Ti I, Ti II, Cr, Ni, Zn, Sr, and Ba as a function of [Fe/H] for the sample of six Boötes I stars (filled circles) and the two comparison field halo stars (open circles). Triangles represent the abundance results from the "GM" analysis in G13, whose systematic offset in the EWs from those in this work is smaller than that in the "NY" analysis.

4.1. Comparison with Feltzing et al. (2009)

Five objects in the present sample have also been studied by F09, who determined Fe, Mg, Ca and Ba abundances for seven objects in Boötes I. The [Fe/H] of the sample stars determined by the present work agree well with the results of F09 within ~ 0.1 dex, except for the lowest metallicity star Boo-094 in our sample, for which the estimated [Fe/H] is -3.4 dex in our study but -2.9 in

F09. This difference can be partly attributed to the higher $\log g$ and larger ξ adopted in our analysis.

The abundances of Mg and Ca also marginally agree with those estimated by F09 within 0.30 dex, except for Boo-127. For this star, F09 report an exceptionally high [Mg/Ca] ratio ([Mg/Ca]> 0.6), while this work has obtained [Mg/Ca]=0.08. The estimated $\log \epsilon$(Mg) in this work is ~ 0.5 dex lower than that reported by F09. Several factors seem to be responsible for the abundance difference, including (1) a higher $\log gf$ value for Mg I 5528 Å (see Table 2), (2) higher $\log g$, and (3) higher ξ in this work than those adopted in F09. While the error in the EWs by up to $\sim 10 - 15$ mÅ may also contribute to the discrepancy, it does not totally explain the large difference.

To illuminate the uncertainty in the $\log gf$ values, we also performed a simple differential analysis to obtain [Mg/Ca] for Boo–127 with respect to one of the comparison stars, HD 217143. Since the $T_{\rm eff}$, $\log g$, and [Fe/H] values are similar between the two stars, a direct comparison of EWs for the Mg I and Ca I lines provides the [Mg/Ca] estimate. Figure 4 shows the wavelength regions that contain the Mg I and Ca I lines for Boo-127 and HD 216143. While both stars show Ca I line with similar strengths, the Boo-127 shows slightly weaker Mg I line than HD 216143, which does not support the anomalously high [Mg/Ca] in Boo-127 compared to the reference star. More quantitatively, The relative abundance $\log(A/A_{\rm ref})$ is expressed as

$$\log\left(\frac{A}{A_{\rm ref}}\right) = \log\left(\frac{EW}{EW_{\rm ref}}\right) - \log\left(\frac{\kappa_\nu}{\kappa_{\nu,{\rm ref}}}\right) - \Delta\theta_{\rm ex}\chi \qquad (1)$$

where κ_ν and $\kappa_{\nu,{\rm ref}}$ are continuum opacity, $\Delta\theta_{\rm ex}$ ($\theta = 5040/T$) is the difference in an excitation temperature, and χ is the excitation potential of the line (Gray 2005). If we assume that the κ_ν term is negligible and $\Delta\theta_{\rm ex}$ is constant and equal to the one computed from the effective temperature ($\Delta\theta_{\rm ex} = \Delta\theta_{\rm ex,eff}$) for all relevant optical depths, the relative abundance can be obtained from the ratios of the EWs (Smith & Harmer 1982). This results in the [Mg/Ca] ratio for Boo–127 being ~ 0.04 dex lower than that of HD 216143, which is, again, inconsistent with the anomalously high [Mg/Ca] ratio. The low, but not extremely low, Ba abundances ([Ba/Fe]~ -0.6) of Boo-121 and Boo-911 found by F09 are confirmed by our measurement. The $\log \epsilon$(Ba) in the two studies agree within 0.3 dex.

4.2. Comparison with Gilmore et al. (2013)

Comparisons of the relative abundances in this work and in the "GM" analysis of G13 are presented in Figure 5 (triangles that are connected with the data points in this work) for the three stars analyzed in common. Within the quoted error bars, our abundance results generally agree with those obtained by G13 with a few exceptions. One relatively large discrepancy is found in the [Fe/H] value for Boo-094, the most metal-poor star in our sample, which is ~ 0.2 dex lower in this work than obtained by G13. The smaller EWs (see Section 2.3) by ~ 10mÅ and larger ξ adopted in this work than in G13 are probably responsible for the discrepancy.

4.3. Carbon

The carbon abundance is estimated for three of the six sample stars, while only an upper limit is obtained for the other three objects. For the six sample stars, extremely carbon-rich objects are not found. These sample stars all show [C/H]< -2.7 and
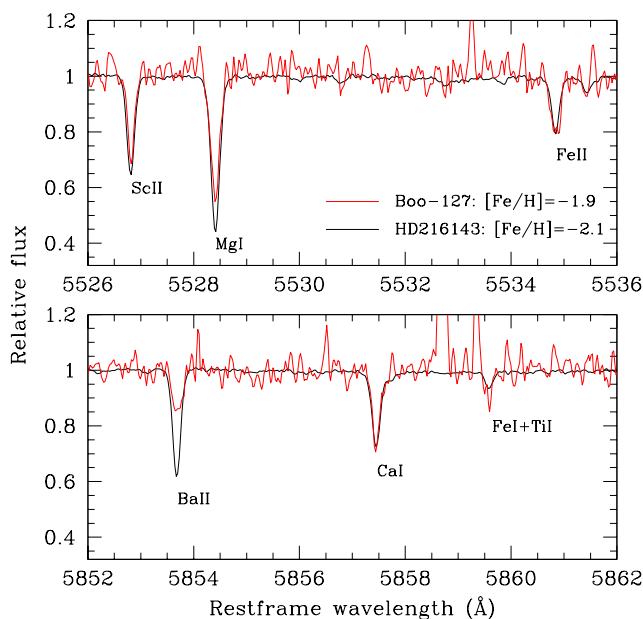
Fig. 4. Spectra of Boo–127(red) and the comparison star, HD 216143 (black), for the wavelength regions that contain Mg I and Ca I lines.

[C/Fe]< 0.2. For the three objects with measured carbon abundances, the average [C/Fe] is −0.7 dex with small scatter. These values are close to the lowest bounds of the [C/Fe] distributions obtained by Lai et al. (2011) and Norris et al. (2010a) for this galaxy. This [C/Fe] value is comparable to what is seen in field halo stars having similar luminosity (Spite et al. 2005; Norris et al. 2010a).

4.4. Sodium

For the present Boötes I sample stars, sodium abundances are only estimated using the strong Na I resonance lines at 5889/5895 Å. These lines are known to suffer from strong non-LTE (NLTE) effects such that LTE abundances tend to be larger than corresponding NLTE values (Takeda et al. 2003). The NLTE correction to Na abundances ranges from −0.1 dex to −0.5 dex, depending on the atmospheric parameters of stars (Takeda et al. 2003). Without any NLTE correction, the average [Na/Fe] value for the six Boötes I stars is ∼ −0.1 dex with small scatter. This value is similar to the uncorrected [Na/Fe] values obtained for field halo stars with comparable metallicities.

4.5. α/Fe ratios

The [Mg/Fe] ratios in our sample stars are similar to or slightly lower than those obtained for the field halo stars. A hint of a modest decreasing trend of the [Mg/Fe] with increasing [Fe/H] is seen, as was also reported in G13. The [Ca/Fe] ratios are also similar to or slightly lower than the value for the field halo stars. Excluding the lowest metallicity star, a scatter in the [Ca/Fe] ratios is remarkably small (∼ 0.1 dex). The [Ti I/Fe I] and [Ti II/Fe II] ratios differ by up to ∼ 0.3 dex in our Boötes I sample stars, as reported for the field halo stars (e.g., Lai et al. 2008). The Boötes I stars tend to show slightly lower [Ti I/Fe small I] abundance ratios than the halo stars, while the [Ti II/Fe II] ratios for these samples are similar.

4.6. Iron-peak elements

Scandium abundances are estimated from a few to several Sc II lines in our sample stars. The mean abundances are similar to or slightly lower than those reported for the field halo stars in [Fe/H]> −2.5.

Chromium abundances are obtained from a few Cr I lines for the Boötes I stars. The [Cr/Fe] ratios are similar to those reported for the field halo stars for two of the most metal-rich stars, while other stars show lower [Cr/Fe] ratios. However, since only one or two lines with low-signal-to-noise ratio are used in the abundance estimate, the significantly lower [Cr/Fe] ratios for these stars require further confirmation.

In the four higher metallicity stars in our sample, the [Ni/Fe] ratios are similar to those obtained for the field halo stars, except for one object (Boo–121). Two Ni I lines used to obtain Ni abundance in this stars both suggest a subsolar [Ni/Fe] ratio.

Since EWs of Zn I lines are not reliably measured for our sample stars, we used spectral synthesis to estimate upper limits of the Zn abundances. The results are shown by bars with downward arrows in the bottom right hand panel of Figure 5. The upper limits of the [Zn/Fe] ratios are similar to or lower than the field halo samples in the metallicity range [Fe/H]> −2.5.

4.7. Neutron-capture elements

The strontium abundances are obtained by fitting synthetic spectra to the observed ones for the Sr II resonance line at 4215.5 Å. The $\log gf$ value for this line is taken from NIST database. Figure 7 shows the resulting synthetic and the observed spectra around the Sr II line for the Boötes I stars for which the Sr abundances are reasonably obtained. The other three sample stars are excluded in the analysis since the spectral region is too noisy to estimate Sr abundances.

In the fitting procedure, we redefine the continuum level using the wavelength regions 4214.10–4215.25 Å and 4216.80–4217.10 Å. To estimate abundance errors due to the uncertainty in the continuum level, we performed the fitting changing the continuum level of the synthetic spectrum by $\pm 1\sigma_{STDV}$, where σ_{STDV} is a standard deviation in the observed continuum level. The error estimated in this procedure is ∼ 0.7 − 1.5 dex, as summarized in Table 5.

For comparison, the bottom panel of Figure 7 shows the observed spectrum of a field halo giant, HD 107752, which has atmospheric parameters similar to those of the present sample (T_{eff}= 4820 K, $\log g$= 1.6, ξ = 1.9 km s^{-1}, and [Fe/H]=−2.8) (Ishigaki et al. 2013). While the Sr II line of the HD 107752 appears to be stronger than a nearby Fe I line, those in the three Boötes I stars seem to have comparable strength as the Fe I lines.

Andrievsky et al. (2011) studied the NLTE effects on Sr abundance determination for extremely metal-poor stars and report that the NLTE correction for the Sr II 4215.5 Å line is at most ~0.2 dex for stars having atmospheric parameters similar to the present Boötes I sample. The correction is smaller than the other sources of uncertainty in the present analysis, so that is not included in our abundance results.

The top panel of Figure 6 shows resulting [Sr/Fe] values plotted against [Fe/H] with the error bars. The crosses and small filled circles represent the abundances from literature extracted from SAGA database and those from Ishigaki et al. (2013), respectively. As can be seen, even though the errors are very large, the [Sr/Fe] ratios of the three Boötes I stars are significantly lower than the solar value, which is not typical for the field halo stars at similar metallicities. Most of the field halo sample in
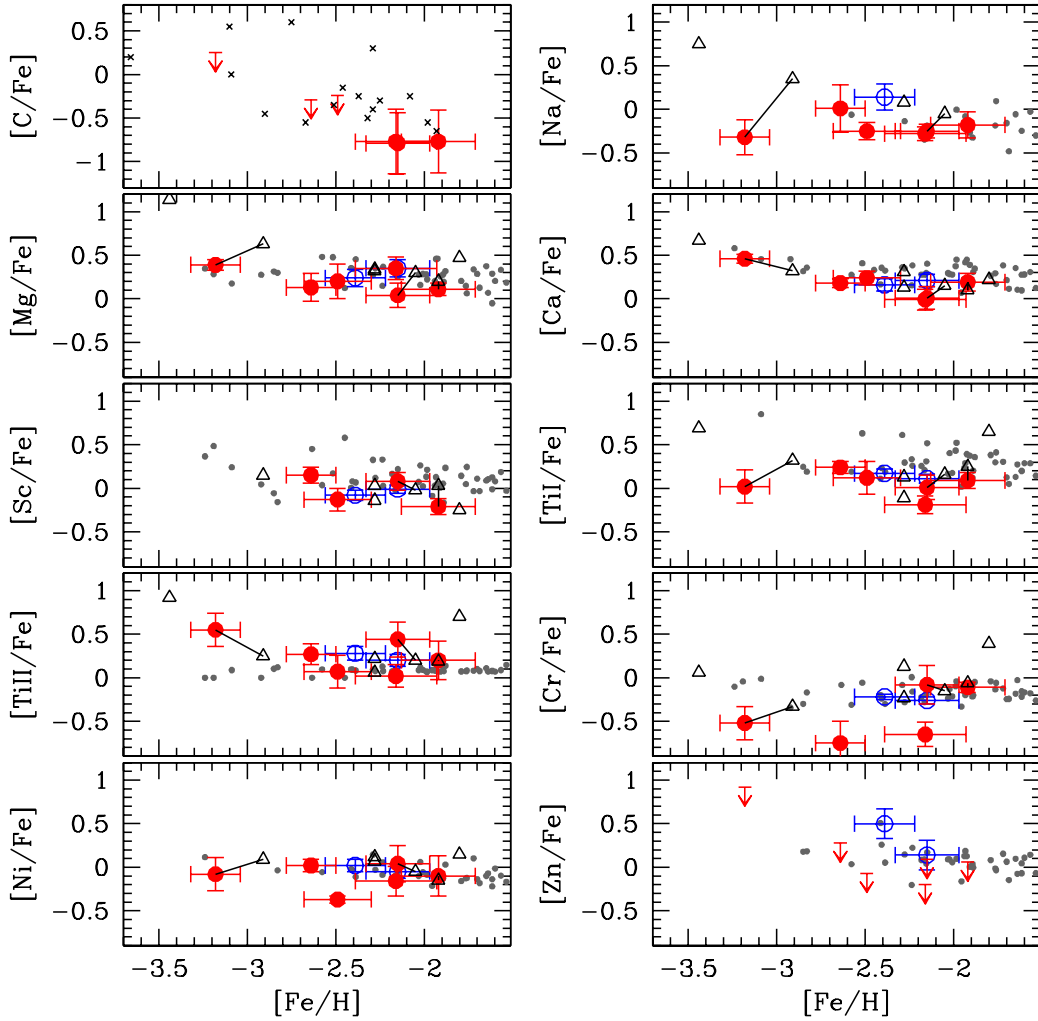
Fig. 5. [X/Fe] ratios plotted against [Fe/H] for the sample of six Boötes I stars (red circles) and the two comparison field halo stars (blue circles). Black triangles represent the abundance results from the "GM" analysis in G13. Small gray circles present the abundances of field halo stars from Ishigaki et al. (2012, 2013). In the plot for [C/Fe]-[Fe/H], results from Norris et al. (2010a) for Boötes I stars are shown in crosses.

literature show the solar value in [Fe/H]< −2.5 and increasing dispersion toward lower metallicity with [Sr/Fe]∼ −2.0 to ∼ 0.5. On the other hand, the Boötes I stars have [Sr/Fe]∼ −1 in [Fe/H]> −2.5, and the most metal-poor star in our sample show even lower [Sr/Fe] of ∼ −2.

The bottom panel of Figure 6 plots the [Ba/Fe] ratios against [Fe/H]. The [Ba/Fe] of Boötes I stars are subsolar, generally confirming the result of G13. The [Ba/Fe] ratios for these stars tend to distribute at the lower bound of the [Ba/Fe] distribution for the field halo stars.

One interesting feature is that Boo–127, which is the most metal-rich star in our sample, shows lower [Ba/Fe] than the field halo stars at similar metallicities ([Fe/H]∼ −2). As shown in Fig 4, the Ba II line is significantly weaker in Boo–127 than seen in the comparison star with similar [Fe/H].

5. Discussion

5.1. Comparison with the field MW halo

If the MW halo was assembled from smaller satellite galaxies similar to the surviving dSphs, as suggested by the standard cosmological model, we naively expect that chemical abundances

in the MW field halo stars are similar to these dSphs. In this section, we address the question of whether the observed abundances in Boötes I stars are similar to those obtained for the field halo stars.

Figure 8 compares mean abundances of the Boötes I stars and field halo stars in the metallicity range of −3.0 <[Fe/H]< −2.0. To minimize systematic errors in the abundance comparison, eight halo giants (T_{eff}< 5000K and log g< 3.0, including one of the comparison stars HD 85773) from Ishigaki et al. (2012, 2013) are only considered for the field halo sample. In their work, the adopted 1D-LTE abundance analysis technique and the line list are the same as in this work. Error bars in Figure 8 represent standard deviations around the mean values.

In comparison to the field halo stars, the Boötes I stars show slightly lower [Mg/Fe] and [Ca/Fe] ratios in the metallicity range of −3.0 <[Fe/H]< −2.0. Kolmogorov-Smirnov (KS) tests suggest that the probability at which [X/Fe] ratios of the halo stars and the Boötes I stars can be drawn from the same distribution is less than 5% for Mg and Ca, which marginally supports the abundance difference. On the other hand, the [Na/Fe] ratios for the Boötes I stars are indistinguishable from those of the halo stars.
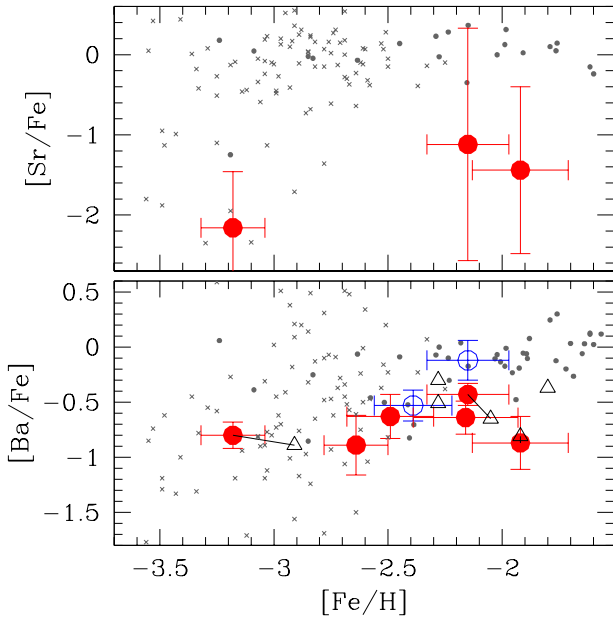
Fig. 6. Same as Figure 5 but for Sr and Ba. Abundance data extracted from the SAGA database (Suda et al. 2008) (RGB, $R > 30000$ with no flags of "C-rich" nor "CEMP") are additionally plotted with gray crosses to supplement the MW halo data.

As mentioned in the previous sections, the Boötes I and the MW halo stars show a hint of an abundance difference in Sr. Figure 9 shows $\log \epsilon(Sr)$ plotted against $\log \epsilon(Ba)$ for the Boötes I stars and MW halo giants. The data for the MW halo giants were
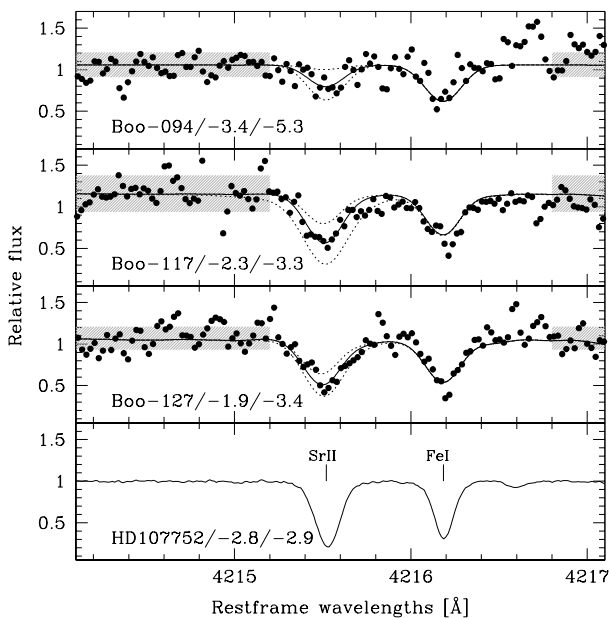

Fig. 7. Observed (black dots) and the best-fit synthetic (solid line) spectra of the three Boötes I stars around the Sr II 4215.5 Å line. The obtained [Fe/H] and [Sr/H] values are indicated in the bottom-left corner of the each panel ("Name/[Fe/H]/[Sr/H]"). The dotted lines show the synthetic spectra fitted after changing the continuum levels by $\pm 1\sigma_{STDV}$ (in each panel, the continuum levels have been shifted to match the best-fit value). For comparison, the spectrum of one halo giant, HD 107752, is shown in the bottom panel.

extracted from the SAGA database (Suda et al. 2008) with criteria, $-3.5 <$[Fe/H]< -2.0 and a spectral resolution $R > 30000$ with no flags of "C-rich" or "CEMP". As can be seen, most of the halo stars show Sr/Ba> 1, while the Boötes I stars show Sr/Ba$\lesssim 1$. Aoki et al. (2005) found that some of the halo stars with [Fe/H]< -3.0 show Sr/Ba> 1, while the excess of Sr is not seen for stars with higher Ba abundances. They interpret the result as evidence that the two astrophysical sites are responsible for producing these neutron-capture elements, one of which produces both Sr and Ba and the other produces more Sr than Ba. Since the signature of enhanced Sr relative to Ba is not evident in our Boötes I sample, the latter astrophysical site may be lacking or less frequent in this galaxy. We discuss the origin of Sr and Ba in Bootes I in Section 5.3.5.

To summarize, the present sample of Boötes I stars show a hint of difference in abundances of some of the α-elements and neutron-capture elements from the bulk of MW halo stars. This result suggests that the chemical abundances of Boötes I stars alone are not enough to fully explain the observed chemical abundances for field halo stars.

Corlies et al. (2013) have investigated conditions that yield a difference in chemical abundances between surviving satellite galaxies and progenitors of the MW halo using an N-body simulation. They suggest that the progenitors of the stellar halo usually experienced more cross pollution by neighboring subhalos, while the surviving satellites tend to have evolved chemically in isolation. Whether the degree of the cross pollution explains the observed abundance difference may have interesting implications for the hierarchical formation of the MW halo.

Since the present result is based on a small sample, a larger sample is clearly desirable to extract a conclusion for the range in elemental abundances spanned by the whole stellar population in Boötes I. Moreover, abundances of field halo stars are often determined only for relatively nearby objects (within a several kpc), while the estimated distance to Boötes I is 64±3 kpc (Okamoto et al. 2012). A systematic abundance survey for more distant halo stars would be needed to examine possible connection between dSphs similar to Boötes I and the MW field halo.

5.2. Comparison with other dSphs

Figure 10 compares the [Mg/Fe] ratios of the Boötes I stars in this work and those of other MW dSphs that include very metal-poor ([Fe/H]< -2) stars from the literature (Aoki et al. 2009; Cohen & Huang 2009, 2010; Frebel et al. 2010; Koch et al. 2008). Relatively luminous ($L_{V,\odot} \gtrsim 10^5 L_\odot$), so-called classical dSphs (Draco, Sextans, Ursa Minor) are shown with green symbols, while less luminous dSphs (UFDs; Boötes I, Coma Berenices, Hercules, Ursa Major II) are shown in red symbols. According to these available data, the more luminous dSphs appear to show relatively low [Mg/Fe] ratios than field halo stars at [Fe/H]~ -2 and/or a decreasing [Mg/Fe] trend with increasing [Fe/H]. On the other hand, the fainter dSphs such as Coma Berenices or Ursa Major II appear to show comparable or higher abundance ratios with large scatter. The Boötes I stars generally show the [Mg/Fe] ratios more similar to some of the classical dSphs, such as Ursa Minor rather than the fainter UFDs, such as Coma Berenices or Ursa Major II, although there seems to be large variation in the abundance ratios among the classical dSphs.

To examine whether the abundance ratios can be related to the global properties of dSphs (e.g., dynamical masses or luminosity), the lower panels in Figure 10 plot average [Mg/Fe] ratios of these dSphs against their central line-of-sight velocity dispersions (σ_{los}; left) and logarithms of total luminosity (L; right).
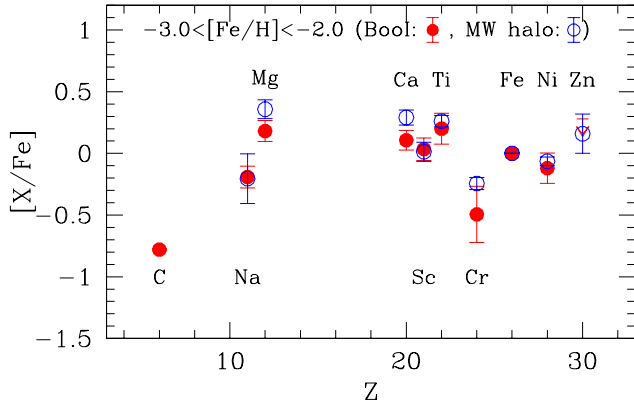
Fig. 8. The abundance pattern of the Boötes I stars (filled circles) and the MW halo stars (open circles) with $-3.0 <$ [Fe/H] < -2.0.
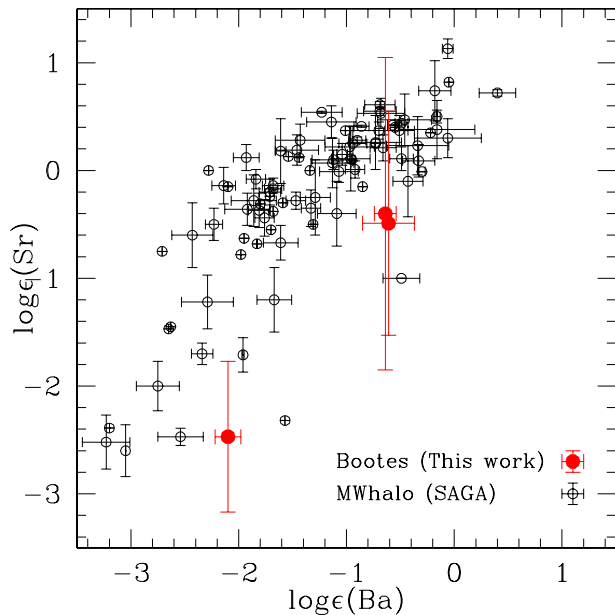

Fig. 9. $\log \epsilon$(Ba) versus $\log \epsilon$(Sr) for the three Boötes I stars. For comparison, the abundance data for MW halo giants are extracted from SAGA database (Suda et al. 2008) with the criteria $-3.5 <$ [Fe/H] < -2.0 and a spectral resolution $R > 30000$ with no flags of "C-rich" or "CEMP".

The data for σ and L are taken from Walker et al. (2009) except for the σ of Boötes I, for which an updated value from Koposov et al. (2011) ($4.6^{+0.8}_{-0.6}$ km s^{-1}, assuming a single component velocity distribution) is available. These figures suggest that the dSphs with larger velocity dispersions or higher luminosity tend to show lower [Mg/Fe] ratios. Again, Boötes I, which has σ as low as that of Coma Berenices and L midway between these two classes of dSphs, show the mean [Mg/Fe] ratio to be more similar to the classical dSphs, such as Ursa Minor or Draco. A similar trend can be seen for [Ca/Fe] ratios as shown in Figure 11.

The exceptionally high [Mg/Fe] ratios are reported for the two Hercules stars, which may suggest an anomalous star formation history for this galaxy (see also François et al. 2012). According to the available data, differences in other elemental abundances lighter than zinc, such as [Na/Fe] ratios, are not very clear among all dSphs including Boötes I for [Fe/H]< -2.

The MW dSphs have been reported to follow a correlation between mean [Fe/H] and L (Kirby et al. 2011b) extending for a wide range of luminosities ($3.5 < \log(L/L_\odot) < 7.5$). Although precision and sample size may not be sufficient to examine the [Mg,Ca/Fe]-σ, -L relation, if any, from currently available data, the locations of Boötes I in these diagrams may have implications for the chemical evolution of this galaxy, which we discuss in Section 5.3

Figure 12 shows [Sr/H] and [Ba/H] ratios plotted against [Fe/H] for Boötes I and other dSphs. Classical dSphs generally show increasing [Sr/H] and [Ba/H] ratios with increasing [Fe/H], similar to the trend seen for field halo stars. On the other hand, the abundances for fainter dSphs tend to distribute at lower bounds than for the field halo stars. Lower abundances of neutron-capture elements for very-metal-poor stars in dSphs have already been noticed in previous studies (e.g., Fulbright et al. 2004; Koch et al. 2008; Frebel et al. 2010; Honda et al. 2011; Koch et al. 2013). Our sample of Boötes I stars show [Ba/H] ratios that are more similar to the classical dSphs, while [Sr/H] ratios are lower, similar to those observed in fainter dSphs.

Whether the neutron-capture elements are more deficient in dSphs than in the MW field halo stars needs to be investigated with a larger sample of high-quality spectra for distant objects, which may be challenging with the current instrumentation. Nevertheless, the detection of Sr and Ba in Boötes I suggests that at least one event that produces neutron-capture elements must have occurred at the earliest epoch of star formation in this galaxy (cf., Roederer 2013).

5.3. Chemical evolution of Boötes I

In Section 5.1, we reported a possible offset in the abundances of α and neutron capture elements between the Boötes I stars and the field halo stars in the metallicity range $-3 <$[Fe/H]< -2. These differences, if confirmed with larger samples, may suggest the differences in chemical evolution history between the Boötes I and dominant progenitors of the MW stellar halo. As discussed in Section 5.2, the [Mg/Fe] and [Ca/Fe] ratios in the observed Boötes I stars are generally similar to the values reported for brighter (classical) dSphs in the metallicity range $-3 <$[Fe/H]< -2, while their velocity dispersion and luminosities are more similar to those of UFDs (Figures 10 and 11).

In this section, we discuss possible implications of the results of these comparisons on the chemical evolution of Boötes I in terms of 1) contribution from Type Ia SNe, 2) galactic winds, 3) tidal interaction with the MW, 4) stochastic effects, and 5) individual supernova yields.

5.3.1. Contribution from Type Ia SNe

In chemical evolution models, trends in abundances of α-elements with [Fe/H] are diagnostics of the Type Ia SNe contribution relative to Type II SNe to chemical enrichments in galaxies (e.g., Matteucci & Greggio 1986). For many of known dSphs, decreasing trends of [α/Fe] with increasing [Fe/H] are reported (Tolstoy et al. 2009; Kirby et al. 2011a; Vargas et al. 2013; Kirby
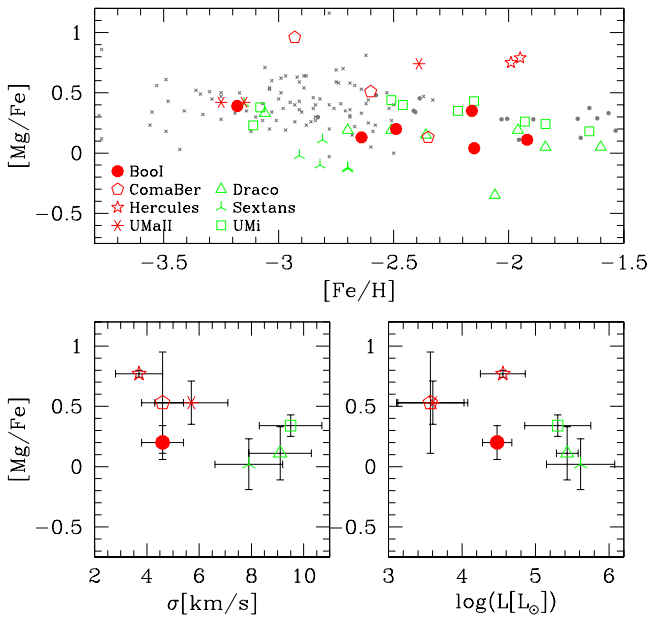
Fig. 10. Top panel: Abundance comparisons with classical (Draco: triangles, Sextans: three pointed asterisk, Ursa Minor: square) and ultrafaint (Coma Berenices: pentagon, Hercules: star, Ursa Major II: asterisk) dwarf galaxies from the literature (Aoki et al. 2009; Cohen & Huang 2009, 2010; Frebel et al. 2010; Koch et al. 2008). For comparison, the abundance data for MW halo giants extracted from SAGA database (Suda et al. 2008) ($R > 30000$ with no flags of "C-rich" or "CEMP") and from Ishigaki et al. (2012) are plotted with crosses and dots, respectively. Bottom panels: Mean [Mg/Fe] ratios for each galaxy plotted against velocity dispersion (σ, left) and luminosity (log $L(L_\odot)$, right) for that galaxy. The σ and L data are taken from Walker et al. (2009).

et al. 2013), which could be indicative of chemical enrichment proceeded partly through Type Ia SNe.

Whether Boötes I has experienced a significant contribution from Type Ia SNe to its chemical enrichments is an important question for constraining the star formation history in this galaxy. Photometric observations suggest that Boötes I is dominated by an old stellar population with little age spread (Okamoto et al. 2012), which suggests that the duration of star formation was shorter than the uncertainty of the photometric age estimates (a few Gyr). Gilmore et al. (2013) suggest a contribution of Type Ia SNe in order to interpret the apparent decreasing [α/Fe] trend with [Fe/H]. On the other hand, the low-resolution spectroscopic study of Lai et al. (2011) does not find a signature of decreasing [α/Fe] ratios with increasing [Fe/H], which does not support the Type Ia contribution.

The observed [Mg/Fe] and [Ca/Fe] ratios for the Boötes I stars in this work appear to show a modest decreasing trend with [Fe/H]. The Pearson test for linear correlation indicates that the probability for a null correlation is 30 % for [Mg/Fe]-[Fe/H] and 7 % for [Ca/Fe]-[Fe/H], thus only marginally supporting the correlation. Although a firm conclusion about the trend could not be obtained for the present sample, the hint of the decreasing trend suggests that the star formation in Boötes I lasted at least until Type Ia SNe began to contribute to the chemical enrichment.

The decreasing [Ca/Fe] trend with [Fe/H] has also been reported for a sample of red giant stars in Hercules dSph, which spans the [Fe/H] range similar to the present Boötes I sample. This may imply that the contribution of Type Ia SNe to the chemical enrichment is common among galaxies as faint as Hercules
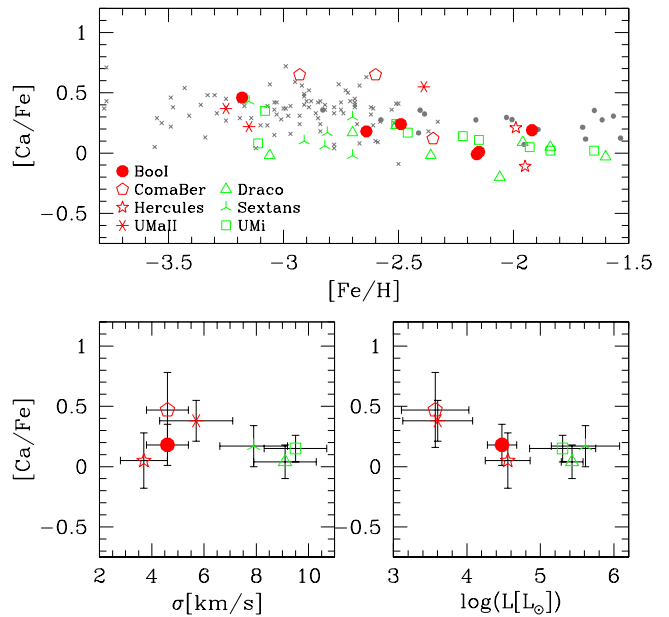
Fig. 11. Same as Figure 10 but for [Ca/Fe].
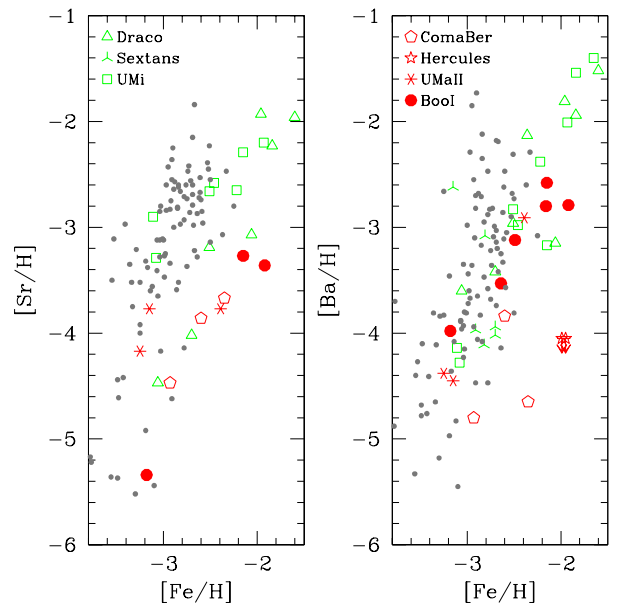
Fig. 12. Comparison of the [Sr/H] and [Ba/H] ratios in Boötes I stars obtained in this work and those in very metal-poor stars in other dSphs. Symbols are the same as in Figure 10.

or Boötes I, if the Type Ia SNe is indeed responsible for lowering [Ca/Fe]. Analyses of the delay-time distribution of Type Ia SNe suggest that a certain fraction of Type Ia SNe occur within < 1 Gyr of star formation (Maoz et al. 2010), which may support their contribution to the chemical enrichments in Boötes I.

An alternative interpretation of the lower [Mg, Ca/Fe] ratios in Boötes I is a different initial mass function (IMF) in this galaxy in comparison to the dominant progenitors of the MW halo. Since [Mg/Fe] yields in Type II SNe could depend on masses of the progenitor stars (Kobayashi et al. 2006), a difference in IMF may lead to systematic difference in these abundance ratios.

5.3.2. Galactic wind

Galactic winds driven by SNe are thought to significantly affect subsequent chemical evolutions in dSphs (Arimoto & Yoshii 1987). Chemical evolution models of Lanfranchi & Matteucci (2004) particularly suggest that the strength and time of occurance of the galactic winds play an important role in determining the [α/Fe] ratios in the dSphs.

The winds are expected to occur when part of the energy injected by SNe heat up interstellar gas so that thermal energy of gas exceed the binding energy of the galaxy (Arimoto & Yoshii 1987). In this scenario, the strength of the wind may depend on both the initial gas content and gravitational potential of the galaxy.

As can be seen in the lower left-hand panels of Figures 10 and 11, the dSphs with smaller velocity dispersion, and thus lower dynamical masses, such as Coma Berenices or Ursa Major II, show higher [Mg/Fe] and [Ca/Fe] ratios than the dSphs with larger velocity dispersions. The likely correlation between the velocity dispersion and the abundance ratios suggests that the chemical abundance depends on the gravitational potential of galaxies, if the velocity dispersion traces the dynamical mass of these systems.

Using the measured velocity dispersion profile, Walker et al. (2009) estimate the dynamical mass of Boötes I within the half-light radius of this galaxy ($r_{\rm half}$ = 242 ± 21 pc) to be $\sim 10^6 M_\odot$. If we assume that the mass has not changed significantly over the age of this galaxy and if duration of star formation is indeed longer than the timescale of Type Ia SNe, as suggested in the previous section, then the above scenario implies that a dark matter halo with mass as low as that of Boötes I could host enough initial gas to retain a certain duration of star formation, or that galactic winds were not strong enough to truncate all subsequent star formation in such a halo. Whether this scenario could be possible depends on the possible tidal effect on the initial gas and dark matter content of this galaxy as discussed below.

5.3.3. Tidal Interaction with the MW

We discussed in Section 5.2 a possible connection of chemical abundance ratios with global properties, such as $\sigma_{\rm los}$ and L. The correlation is not currently clear, and Boötes I in particular appears to deviate from a possible relation. Thus, we may ask what makes Boötes I smaller $\sigma_{\rm los}$ and lower L, while experiencing chemical evolution that is more like the brighter classical dSphs.

One possible mechanism that may affect $\sigma_{\rm los}$ or L is tidal interaction with the MW potential. Tidal interaction of Boötes I with the MW may have stripped the original content of baryons and dark matter in this galaxy. N-body simulations for dynamical evolution of Boötes I suggest that this galaxy has lost a significant amount of luminous and dark matter contents by the tidal forces as it orbits around the MW potential (Fellhauer et al. 2008). It is possible that Boötes I was initially as luminous as the classical dSphs, while it has lost a significant amount of materials.

Since the full orbital motion of Boötes I is not known, it is difficult to estimate how strong the tidal effects were in this galaxy. The tidal radius of this galaxy at its present location (62 kpc from the Galactic center) is estimated to be 1.2 kpc (Fellhauer et al. 2008), which is larger than the luminous component in this galaxy. Therefore, it is unlikely that the tidal effect is currently significant in stripping material from this galaxy. On the other hand, Collins et al. (2013) report that the estimated maximum circular velocity ($V_{\rm max}$) for Boötes I is relatively low compared to other local group dSphs with wide ranges of luminosities, which could be explained by tidal stripping of dark matter. Therefore, one explanation of the observed similarity may be that Boötes I once experienced similar chemical evolution to, say, Ursa Minor, then within a few Gyr, it followed an orbit that brought it closer to the Galactic center, experiencing strong tidal force that were able to strip luminous and dark matter contents in this galaxy. All subsequent star formation stopped, which results in the current low luminosity and very low metallicity ([Fe/H]< −1.5) in this galaxy (Norris et al. 2010a). The information about the orbital motion of Boötes I would be necessary for examining such a scenario to interpret the observed chemical abundances in this galaxy.

5.3.4. Stochastic effect

In very low-metallicity systems like Boötes I, it is possible that only a small number of SNe of a prior generation of stars have contributed to the chemical enrichment. For example, Frebel & Bromm (2012) suggest that first galaxies that formed exclusively from ejecta of the first generation of stars (Pop III stars) are expected to host relatively few progenitor SNe, which could be around ten, compared to systems with higher metallicity. In this case, the effects of stochastic sampling of an IMF may become important.

The present sample of Boötes I stars are rather homogeneous in abundance ratios for elements lighter than zinc, which does not strongly support the existence of any stochastic effect. Nevertheless, the observed homogeneous [X/Fe] ratios do not completely rule out the stochastic enrichment scenario, since little scatter in [X/Fe] is expected, while producing large scatter in [Fe/H] in such scenarios as proposed by Frebel & Bromm (2012). This scenario thus implies that Boötes I could be a candidate for the first galaxies formed in the Universe.

Lee et al. (2013) have recently investigated the effect of the stochastic IMF sampling as a possible interpretation of the abundance difference and similarity between the UFDs and MW halo stars. In their model, a system enriched by a smaller number of a prior generation of stars is expected to show a lower mean value of [X/Fe] with larger spread, when the supernova yield of an element X has a positive mass dependence (i.e., higher ejected mass for a higher supernova progenitor mass). Therefore, if a UFD has been enriched by fewer SNe ($\sim 1 − 7$ on average) than the progenitors of the MW halo (> 7) and if a Sr yield, which is currently uncertain, has a strong positive mass dependence, we would expect lower [Sr/Fe] for the UFDs than the MW halo progenitor. They conclude that the stochastic sampling of IMF for UFDs can simultaneously explain the observed difference in [Sr, Ba/Fe] ratios and the similarity in [Ti/Fe] ratios between the UFDs and MW halo stars.

The result of the present work, a modest difference in [Mg/Fe] and a large difference in [Sr/Fe] from field halo stars appear to both be reproduced with the above model if the Sr yield depends more strongly on progenitor masses than the Mg yields do. Thus, according to this model, the difference in number of prior-generation stars can explain the observed abundance difference between the Boötes I and progenitors of the MW halo.

5.3.5. Individual yields

We finally discuss whether the abundances of the present sample stars are consistent with yields of a single SN of Pop III stars. Pop III stars may have been very massive. Very massive stars

with M> $140 M_\odot$ are predicted to be exploded as pair-instability SNe whose yields are expected to show a peculiar abundance pattern, including very large Ca abundances. As can be seen, none of our sample stars show this peculiar pattern and seem to be more consistent with yields of core-collapse SNe (e.g., Tominaga et al. 2007).

An intriguing issue is whether nucleosynthetic yields of SNe are compatible with the observed abundances of Sr and Ba in Boötes I. Core-collapse SNe of massive ($> 10 M_\odot$) stars have been considered as one of the promising production sites of heavy neutron-capture elements such as Ba (e.g., Thielemann et al. 2011). However, more recent studies report difficulty in reproducing the required physical condition for the r-process to occur in the environment of the core-collapse SNe.

Qian & Wasserburg (2008) used the phenomenological model to study nucleosynthetic yields of neutron-capture elements in neutrino-driven winds, which are associated with SNe. They pointed out that the low [Sr/Fe] ratios are not reproduced with the predicted yields of Type II SNe with progenitor masses of neither $8 - 10 M_\odot$ (H source) nor $12 - 25 M_\odot$ (L sources). Instead, they suggest that another source that produces a large amount of Fe but little Sr is required to explain the abundance patterns of stars with [Sr/Fe]$<< -0.32$. They speculate that an energetic SN, a so-called hypernova, could be a possible astrophysical site that yields the low [Sr/Fe] ratios. In this scenario, the observed Boötes I stars may have formed out of interstellar medium predominantly enriched by a single supernovae with large explosion energy.

A merging of neutron stars in a close binary system is proposed as an alternative site of the r-process. Recent calculations of nucleosynthetic yields for the neutron-star merger successfully explain the abundance patterns of known r-process-rich stars in the Galactic field halo (e.g., Wanajo & Janka 2012; Korobkin et al. 2012). It is interesting for future studies to investigate whether the predicted nucleosynthetic yields of neutron star mergers can explain the observed Sr/Fe and/or Ba/Fe abundances in Boötes I.

The supernova yields depend on various unknown parameters, such as mass cut or explosion energies, and thus properties of the progenitor SN are not fully constrained at this moment. Nucleosynthetic yields of light and heavy neutron capture elements for different SN progenitor masses at extremely low metallicities are required to examine the reason for the Sr deficiency in Boötes I.

6. Conclusions

The chemical abundances of C, Na, α, iron-peak, and neutron capture elements in six giant stars in Boötes I ultra-faint dwarf galaxy were estimated based on the high-resolution spectra obtained with Subaru/HDS. Our main results are summarized as follows:

1. The very low metallicity of Boo–094 ([Fe/H]= -3.4) previously reported in Feltzing et al. (2009) and Gilmore et al. (2013) is confirmed. For the six sample stars, extremely carbon-rich objects are not found.
2. For α and iron-peak elements, the scatter in the abundance ratios is small over the metallicity range of -2.7 <[Fe/H]< -1.8.
3. The [Mg/Fe] and [Ca/Fe] ratios for these stars are slightly lower than the field halo stars on average in the metallicity range of -3.0 <[Fe/H]< -2.0. On the other hand, the abundance ratios for Na and Sc in the Boötes I stars are generally similar to those of the field halo stars.

4. The [Sr/Fe] abundances of the three Boötes I stars are lower than the field halo values at similar metallicities. These Boötes I stars deviate from the correlation between $\log \epsilon(\mathrm{Ba})$ and $\log \epsilon(\mathrm{Sr})$ seen in field MW halo stars and generally show lower Sr/Ba ratios.

Highly inhomogeneous chemical abundances that are reported in fainter dSphs are not seen in our Boötes I sample. Instead, our results suggest that the star formation in Boötes I had lasted until Type Ia SNe started to contribute to the chemical enrichment, which has also been reported in other more luminous dSphs. Larger samples of chemical abundances and the kinematics of individual stars, as well as a determination of the orbital motion around the MW, are desirable to conclude whether Boötes I is once more similar to brighter dSphs or is a surviving example of first galaxies formed out of ejecta from Pop III stars.

References

Aldenius, M., Tanner, J. D., Johansson, S., Lundberg, H., & Ryan, S. G. 2007, A&A, 461, 767
Andrievsky, S. M., Spite, F., Korotin, S. A., et al. 2011, A&A, 530, A105
Aoki, W., Arimoto, N., Sadakane, K., et al. 2009, A&A, 502, 569
Aoki, W., Honda, S., Beers, T. C., et al. 2005, ApJ, 632, 611
Arimoto, N. & Yoshii, Y. 1987, A&A, 173, 23
Asplund, M., Grevesse, N., Sauval, A. J., & Scott, P. 2009, ARA&A, 47, 481
Belokurov, V., Zucker, D. B., Evans, N. W., et al. 2006, ApJ, 647, L111
Cayrel, R. 1988, in IAU Symposium, Vol. 132, The Impact of Very High S/N Spectroscopy on Stellar Physics, ed. G. Cayrel de Strobel & M. Spite, 345
Cohen, J. G. & Huang, W. 2009, ApJ, 701, 1053
Cohen, J. G. & Huang, W. 2010, ApJ, 719, 931
Collins, M. L. M., Chapman, S. C., Rich, R. M., et al. 2013, ArXiv e-prints
Corlies, L., Johnston, K. V., Tumlinson, J., & Bryan, G. 2013, ArXiv e-prints
Demarque, P., Woo, J.-H., Kim, Y.-C., & Yi, S. K. 2004, ApJS, 155, 667
Fellhauer, M., Wilkinson, M. I., Evans, N. W., et al. 2008, MNRAS, 385, 1095
Feltzing, S., Eriksson, K., Kleyna, J., & Wilkinson, M. I. 2009, A&A, 508, L1
François, P., Monaco, L., Villanova, S., et al. 2012, in American Institute of Physics Conference Series, ed. S. Kubono, T. Hayakawa, T. Kajino, H. Miyatake, T. Motobayashi, & K. Nomoto, Vol. 1484, 460–462
Frebel, A. & Bromm, V. 2012, ApJ, 759, 115
Frebel, A., Simon, J. D., Geha, M., & Willman, B. 2010, ApJ, 708, 560
Fulbright, J. P., Rich, R. M., & Castro, S. 2004, ApJ, 612, 447
Gilmore, G., Norris, J. E., Monaco, L., et al. 2013, ApJ, 763, 61
Gray, D. F. 2005, The Observation and Analysis of Stellar Photospheres (The Edinburgh Buiding, Cambridge CB2 2RU, UK: Cambridge University Press)
Honda, S., Aoki, W., Arimoto, N., & Sadakane, K. 2011, PASJ, 63, 523
Ishigaki, M. N., Aoki, W., & Chiba, M. 2013, ApJ, 771, 67
Ishigaki, M. N., Chiba, M., & Aoki, W. 2012, ApJ, 753, 64
Kirby, E. N., Boylan-Kolchin, M., Cohen, J. G., et al. 2013, ApJ, 770, 16
Kirby, E. N., Cohen, J. G., Smith, G. H., et al. 2011a, ApJ, 727, 79
Kirby, E. N., Lanfranchi, G. A., Simon, J. D., Cohen, J. G., & Guhathakurta, P. 2011b, ApJ, 727, 78
Kobayashi, C., Umeda, H., Nomoto, K., Tominaga, N., & Ohkubo, T. 2006, ApJ, 653, 1145
Koch, A., Feltzing, S., Adén, D., & Matteucci, F. 2013, A&A, 554, A5
Koch, A., McWilliam, A., Grebel, E. K., Zucker, D. B., & Belokurov, V. 2008, ApJ, 688, L13
Koposov, S. E., Gilmore, G., Walker, M. G., et al. 2011, ApJ, 736, 146
Korobkin, O., Rosswog, S., Arcones, A., & Winteler, C. 2012, MNRAS, 426, 1940
Lai, D. K., Bolte, M., Johnson, J. A., et al. 2008, ApJ, 681, 1524
Lai, D. K., Lee, Y. S., Bolte, M., et al. 2011, ApJ, 738, 51
Lanfranchi, G. A. & Matteucci, F. 2004, MNRAS, 351, 1338
Lee, D. M., Johnston, K. V., Tumlinson, J., Sen, B., & Simon, J. D. 2013, ArXiv e-prints
Maoz, D., Sharon, K., & Gal-Yam, A. 2010, ApJ, 722, 1879

Martin, N. F., Ibata, R. A., Chapman, S. C., Irwin, M., & Lewis, G. F. 2007, MNRAS, 380, 281
Matteucci, F. & Greggio, L. 1986, A&A, 154, 279
McWilliam, A. 1998, AJ, 115, 1640
Muñoz, R. R., Carlin, J. L., Frinchaboy, P. M., et al. 2006, ApJ, 650, L51
Noguchi, K., Aoki, W., Kawanomoto, S., et al. 2002, PASJ, 54, 855
Norris, J. E., Gilmore, G., Wyse, R. F. G., et al. 2008, ApJ, 689, L113
Norris, J. E., Wyse, R. F. G., Gilmore, G., et al. 2010a, ApJ, 723, 1632
Norris, J. E., Yong, D., Gilmore, G., & Wyse, R. F. G. 2010b, ApJ, 711, 350
Okamoto, S., Arimoto, N., Yamada, Y., & Onodera, M. 2012, ApJ, 744, 96
Qian, Y.-Z. & Wasserburg, G. J. 2008, ApJ, 687, 272
Roederer, I. U. 2013, AJ, 145, 26
Schlafly, E. F. & Finkbeiner, D. P. 2011, ApJ, 737, 103
Schlegel, D. J., Finkbeiner, D. P., & Davis, M. 1998, ApJ, 500, 525
Smith, G. R. & Harmer, D. L. 1982, MNRAS, 198, 273
Spite, M., Cayrel, R., Plez, B., et al. 2005, A&A, 430, 655
Suda, T., Katsuta, Y., Yamada, S., et al. 2008, PASJ, 60, 1159
Takeda, Y., Zhao, G., Takada-Hidai, M., et al. 2003, Chinese J. Astron. Astrophys., 3, 316
Thielemann, F.-K., Arcones, A., Käppeli, R., et al. 2011, Progress in Particle and Nuclear Physics, 66, 346
Tolstoy, E., Hill, V., & Tosi, M. 2009, ARA&A, 47, 371
Tominaga, N., Umeda, H., & Nomoto, K. 2007, ApJ, 660, 516
Vargas, L. C., Geha, M., Kirby, E. N., & Simon, J. D. 2013, ApJ, 767, 134
Walker, M. G., Mateo, M., Olszewski, E. W., et al. 2009, ApJ, 704, 1274
Wanajo, S. & Janka, H.-T. 2012, ApJ, 746, 180
York, D. G., Adelman, J., Anderson, Jr., J. E., et al. 2000, AJ, 120, 1579

Table 4. Equivalent widths and abundances. Table 4 is published in its entirety in the electronic edition of the Astronomy & Astrophysics. A portion is shown here for guidance regarding its form and context.

Object	Elem.	Ion	Wavelength (Å)	χ (eV)	$\log gf$	EW (mÅ)	$\log \epsilon A$ (dex)
Boo–009	11	1	5895.92	0.00	−0.19	150.0	3.61
Boo–009	12	1	4702.99	4.35	−0.44	50.1	4.94
Boo–009	12	1	5528.40	4.35	−0.50	69.7	5.24

Table 5. Elemental abundances and uncertainties

Name	Elem.	$\log \epsilon A_\odot$	$\log \epsilon A$	[X/H]	[X/Fe]	N	σ_{line}	Δ^{+100K}_{-100K}	$\Delta^{+0.3\text{dex}}_{-0.3\text{dex}}$	$\Delta^{+0.3\text{kms}^{-1}}_{-0.3\text{kms}^{-1}}$	σ_{tot}
Boo–009	FeI	7.50	4.86	−2.64	−2.64	38	0.04	0.12 / −0.12	−0.02 / 0.03	−0.04 / 0.06	0.14
	FeII	7.50	4.59	−2.91	−2.91	2	0.01	0.01 / 0.00	0.10 / −0.09	−0.01 / 0.02	0.10
	C(CH)	8.43	< 5.50	< −2.93	< −0.29	1	...	...	...	...	...
	NaI	6.24	3.61	−2.63	0.01	1	0.25	0.01 / −0.01	−0.03 / 0.02	−0.10 / 0.10	0.27
	MgI	7.60	5.09	−2.51	0.13	2	0.15	−0.06 / 0.06	0.00 / −0.00	0.01 / −0.02	0.16
	CaI	6.34	3.88	−2.46	0.18	2	0.04	0.06 / −0.03	−0.00 / 0.00	−0.01 / 0.00	0.05
	ScII	3.15	0.39	−2.76	0.15	2	0.09	0.04 / −0.04	−0.00 / 0.01	−0.00 / 0.00	0.09
	TiI	4.95	2.56	−2.39	0.24	2	0.07	0.01 / −0.01	−0.00 / 0.00	0.02 / −0.02	0.07
	TiII	4.95	2.31	−2.64	0.27	2	0.11	0.04 / −0.04	−0.01 / 0.01	−0.02 / 0.03	0.12
	CrI	5.64	2.25	−3.39	−0.75	1	0.25	...	0.00 / −0.00	...	0.25
	NiI	6.22	3.60	−2.62	0.02	2	0.07	0.00 / −0.00	0.00 / −0.01	0.01 / −0.01	0.07
	ZnI	4.56	< 2.20	< −2.36	< 0.28	1	...	...	...	...	...
	SrII	2.87	...	...	...	0	...	...	...	...	...
	BaII	2.18	−1.61	−3.79	−0.89	1	0.25	0.08 / −0.08	−0.01 / 0.01	−0.02 / 0.02	0.27
Boo–094	FeI	7.50	4.32	−3.18	−3.18	22	0.04	0.12 / −0.12	−0.04 / 0.04	−0.02 / 0.03	0.14
	FeII	7.50	4.02	−3.48	−3.48	2	0.16	...	0.09 / −0.08	−0.03 / 0.03	0.19
	C(CH)	8.43	< 5.50	< −2.93	< 0.25	1	...	...	...	...	...
	NaI	6.24	2.73	−3.51	−0.32	1	0.19	−0.01 / 0.00	−0.01 / 0.01	−0.07 / 0.08	0.20
	MgI	7.60	4.81	−2.79	0.39	3	0.05	−0.03 / 0.03	0.00 / −0.00	0.01 / −0.01	0.06
	CaI	6.34	3.61	−2.73	0.46	2	0.01	−0.04 / 0.05	0.01 / −0.01	0.01 / −0.01	0.05
	ScII	3.15	...	...	...	0	...	...	...	...	...
	TiI	4.95	1.79	−3.16	0.02	1	0.19	0.01 / −0.01	0.00 / −0.00	0.01 / −0.02	0.19
	TiII	4.95	2.02	−2.93	0.55	1	0.19	0.04 / −0.04	−0.00 / −0.00	0.02 / −0.03	0.19
	CrI	5.64	1.94	−3.70	−0.52	1	0.19	0.00 / −0.00	−0.00 / 0.00	−0.00 / 0.00	0.19
	NiI	6.22	2.96	−3.26	−0.08	1	0.19	−0.00 / 0.00	0.00 / −0.00	0.00 / −0.00	0.19
	ZnI	4.56	< 2.30	< −2.26	< 0.92	1	...	...	...	...	...
	SrII	2.87	−2.47	−5.34	−2.16	1	0.70	...	...	...	0.70
	BaII	2.18	−2.10	−4.28	−0.80	3	0.10	0.07 / −0.08	−0.01 / 0.01	0.01 / −0.01	0.12
Boo–117	FeI	7.50	5.35	−2.15	−2.15	32	0.04	0.13 / −0.13	−0.03 / 0.03	−0.10 / 0.13	0.18
	FeII	7.50	5.11	−2.39	−2.39	3	0.14	0.00 / 0.01	0.10 / −0.10	−0.04 / 0.05	0.18
	C(CH)	8.43	5.49	−2.94	−0.79	1	0.30	−0.13 / 0.13	0.03 / −0.03	0.10 / −0.13	0.35
	NaI	6.24	3.84	−2.40	−0.25	2	0.05	0.02 / −0.02	−0.05 / 0.04	−0.05 / 0.02	0.08
	MgI	7.60	5.50	−2.10	0.04	3	0.13	−0.03 / 0.03	−0.00 / 0.00	0.03 / −0.05	0.14
	CaI	6.34	4.21	−2.13	0.01	6	0.11	−0.04 / 0.05	0.01 / −0.01	0.05 / −0.07	0.13
	ScII	3.15	0.85	−2.30	0.08	3	0.09	0.04 / −0.04	−0.00 / 0.00	0.01 / −0.01	0.10
	TiI	4.95	2.81	−2.14	0.01	3	0.13	0.01 / −0.00	0.00 / −0.00	0.04 / −0.06	0.14
	TiII	4.95	3.00	−1.95	0.44	1	0.20	0.04 / −0.04	−0.00 / 0.01	−0.02 / 0.03	0.20
	CrI	5.64	3.41	−2.23	−0.08	1	0.20	−0.01 / 0.02	0.01 / −0.01	0.08 / −0.10	0.22
	NiI	6.22	4.11	−2.11	0.04	1	0.20	0.01 / −0.01	−0.01 / 0.01	−0.06 / 0.07	0.21
	ZnI	4.56	< 2.50	< −2.06	< 0.09	1	...	...	...	...	...
	SrII	2.87	−0.40	−3.27	−1.12	1	1.45	...	...	...	1.45
	BaII	2.18	−0.64	−2.82	−0.43	2	0.05	0.07 / −0.07	−0.00 / 0.00	−0.03 / 0.05	0.10
Boo–121	FeI	7.50	5.01	−2.49	−2.49	34	0.03	0.15 / −0.16	−0.05 / 0.05	−0.08 / 0.11	0.19
	FeII	7.50	4.89	−2.61	−2.61	4	0.07	−0.00 / 0.02	0.09 / −0.08	−0.06 / 0.08	0.13
	C(CH)	8.43	< 5.70	< −2.73	< −0.24	1	...	...	...	...	...
	NaI	6.24	3.50	−2.74	−0.25	2	0.05	0.03 / −0.05	−0.03 / 0.02	−0.08 / 0.05	0.10
	MgI	7.60	5.31	−2.29	0.20	1	0.18	0.09 / −0.08	0.00 / −0.00	0.02 / −0.04	0.20

Table 5. continued.

Name	Elem.	$\log \epsilon A_\odot$	$\log \epsilon A$	[X/H]	[X/Fe]	N	σ_{line}	Δ^{+100K}_{-100K}	$\Delta^{+0.3\text{dex}}_{-0.3\text{dex}}$	$\Delta^{+0.3\text{kms}^{-1}}_{-0.3\text{kms}^{-1}}$	σ_{tot}
	CaI	6.34	4.09	−2.25	0.24	4	0.06	−0.05 / 0.05	0.00 / −0.01	0.02 / −0.02	0.08
	ScII	3.15	0.41	−2.73	−0.13	3	0.11	0.04 / −0.04	0.00 / −0.01	0.04 / −0.05	0.13
	TiI	4.95	2.59	−2.36	0.12	2	0.19	0.01 / −0.02	−0.00 / 0.01	0.03 / −0.03	0.19
	TiII	4.95	2.41	−2.54	0.07	1	0.18	0.04 / −0.04	0.00 / −0.00	0.03 / −0.04	0.19
	CrI	5.64	...	...	...	0	...	...	...	...	...
	NiI	6.22	3.36	−2.86	−0.37	2	0.02	−0.00 / 0.01	0.01 / −0.01	0.03 / −0.04	0.04
	ZnI	4.56	< 2.00	< −2.56	< −0.07	1	...	...	...	...	...
	SrII	2.87	...	...	...	0	...	...	...	...	...
	BaII	2.18	−1.06	−3.24	−0.63	1	0.18	0.07 / −0.08	0.00 / −0.01	−0.01 / 0.02	0.20
Boo–127	FeI	7.50	5.58	−1.92	−1.92	42	0.03	0.15 / −0.15	−0.03 / 0.03	−0.12 / 0.14	0.21
	FeII	7.50	5.58	−1.92	−1.92	6	0.07	−0.01 / 0.02	0.10 / −0.10	−0.10 / 0.13	0.17
	C(CH)	8.43	5.74	−2.69	−0.77	1	0.30	−0.15 / 0.15	0.03 / −0.03	0.12 / −0.14	0.36
	NaI	6.24	4.14	−2.10	−0.18	2	0.14	0.02 / −0.02	−0.06 / 0.06	−0.02 / −0.02	0.15
	MgI	7.60	5.79	−1.81	0.11	2	0.01	−0.06 / 0.06	−0.02 / 0.02	0.02 / −0.04	0.07
	CaI	6.34	4.61	−1.73	0.19	5	0.09	−0.04 / 0.04	−0.01 / 0.00	0.02 / −0.03	0.10
	ScII	3.15	1.02	−2.13	−0.21	3	0.05	0.03 / −0.04	0.00 / 0.00	0.06 / −0.08	0.09
	TiI	4.95	3.12	−1.83	0.09	4	0.09	0.02 / −0.02	−0.00 / 0.01	−0.01 / 0.02	0.09
	TiII	4.95	3.23	−1.72	0.20	1	0.22	0.03 / −0.04	−0.00 / 0.00	0.01 / −0.01	0.22
	CrI	5.64	3.61	−2.03	−0.11	2	0.04	−0.01 / 0.00	0.00 / −0.00	0.05 / −0.05	0.06
	NiI	6.22	4.21	−2.02	−0.10	1	0.22	0.02 / −0.01	−0.01 / 0.01	−0.07 / 0.08	0.23
	ZnI	4.56	< 2.70	< −1.86	< 0.06	1	...	...	...	...	...
	SrII	2.87	−0.49	−3.36	−1.44	1	1.04	...	...	...	1.04
	BaII	2.18	−0.61	−2.79	−0.87	1	0.22	0.06 / −0.06	0.01 / −0.01	0.07 / −0.09	0.24
Boo–911	FeI	7.50	5.34	−2.16	−2.16	26	0.02	0.17 / −0.18	−0.04 / 0.05	−0.12 / 0.15	0.23
	FeII	7.50	5.32	−2.18	−2.18	2	0.06	−0.02 / 0.03	0.09 / −0.08	−0.12 / 0.16	0.18
	C(CH)	8.43	5.50	−2.93	−0.77	1	0.30	−0.17 / 0.18	0.04 / −0.05	0.12 / −0.15	0.37
	NaI	6.24	3.80	−2.44	−0.28	2	0.05	0.04 / −0.05	−0.03 / 0.03	−0.05 / 0.00	0.08
	MgI	7.60	5.79	−1.81	0.35	1	0.11	−0.07 / 0.08	−0.02 / 0.02	0.00 / −0.02	0.13
	CaI	6.34	4.17	−2.17	−0.01	5	0.09	−0.06 / 0.06	0.00 / −0.01	0.04 / −0.06	0.12
	ScII	3.15	...	...	...	0	...	...	...	...	...
	TiI	4.95	2.60	−2.35	−0.19	5	0.08	0.02 / −0.03	−0.00 / 0.00	0.05 / −0.06	0.10
	TiII	4.95	2.79	−2.16	0.02	1	0.11	0.04 / −0.04	...	0.04 / −0.06	0.13
	CrI	5.64	2.83	−2.81	−0.65	1	0.11	0.03 / −0.04	−0.02 / 0.02	0.08 / −0.07	0.14
	NiI	6.22	3.90	−2.32	−0.16	3	0.17	−0.02 / 0.03	0.01 / −0.01	0.03 / −0.04	0.17
	ZnI	4.56	< 2.20	< −2.36	< −0.20	1	...	...	...	...	...
	SrII	2.87	...	...	...	0	...	...	...	...	...
	BaII	2.18	−0.64	−2.82	−0.64	3	0.12	0.08 / −0.08	0.01 / −0.01	−0.02 / 0.03	0.15
HD216143	FeI	7.50	5.35	−2.15	−2.15	64	0.01	0.15 / −0.16	−0.03 / 0.03	−0.07 / 0.09	0.18
	FeII	7.50	5.35	−2.15	−2.15	13	0.01	−0.02 / 0.03	0.11 / −0.10	−0.04 / 0.05	0.12
	C(CH)	8.43	...	...	...	0	...	...	...	...	...
	NaI	6.24	...	...	...	0	...	...	...	...	...
	MgI	7.60	5.80	−1.80	0.35	2	0.07	−0.05 / 0.05	−0.04 / 0.04	−0.03 / 0.02	0.10
	CaI	6.34	4.40	−1.94	0.21	16	0.03	−0.05 / 0.05	−0.00 / 0.00	0.03 / −0.04	0.07
	ScII	3.15	0.99	−2.16	−0.01	8	0.03	0.04 / −0.04	−0.00 / 0.00	0.01 / −0.01	0.05
	TiI	4.95	2.92	−2.04	0.11	18	0.03	0.02 / −0.03	−0.01 / 0.00	0.03 / −0.04	0.05
	TiII	4.95	3.00	−1.95	0.20	6	0.04	0.03 / −0.04	−0.01 / 0.01	−0.04 / 0.05	0.07
	CrI	5.64	3.23	−2.41	−0.26	4	0.03	0.01 / −0.01	−0.01 / 0.01	0.02 / −0.02	0.04
	NiI	6.22	4.02	−2.20	−0.05	12	0.02	−0.04 / 0.05	0.02 / −0.02	0.05 / −0.07	0.08
	ZnI	4.56	2.55	−2.01	0.14	2	0.01	−0.13 / 0.16	0.09 / −0.09	0.04 / −0.05	0.17
	SrII	2.87	...	...	...	0	...	...	...	...	...
	BaII	2.18	−0.09	−2.27	−0.12	3	0.06	0.07 / −0.09	−0.01 / 0.01	−0.13 / 0.16	0.18
HD85773	FeI	7.50	5.11	−2.39	−2.39	58	0.01	0.14 / −0.16	−0.04 / 0.04	−0.06 / 0.07	0.17
	FeII	7.50	5.17	−2.33	−2.33	12	0.01	−0.02 / 0.03	0.10 / −0.10	−0.03 / 0.04	0.11
	C(CH)	8.43	...	...	...	0	...	...	...	...	...
	NaI	6.24	3.99	−2.25	0.14	1	0.11	−0.08 / 0.09	0.02 / −0.02	0.05 / −0.07	0.15
	MgI	7.60	5.45	−2.15	0.24	3	0.08	−0.07 / 0.07	0.01 / −0.02	−0.00 / −0.01	0.10
	CaI	6.34	4.11	−2.23	0.16	16	0.02	−0.05 / 0.05	0.00 / −0.01	0.02 / −0.03	0.07

Table 5. continued.

Name	Elem.	$\log \epsilon A_\odot$	$\log \epsilon A$	[X/H]	[X/Fe]	N	σ_{line}	$\Delta^{+100\text{K}}_{-100\text{K}}$	$\Delta^{+0.3\text{dex}}_{-0.3\text{dex}}$	$\Delta^{+0.3\text{kms}^{-1}}_{-0.3\text{kms}^{-1}}$	σ_{tot}
	ScII	3.15	0.74	−2.41	−0.08	6	0.03	0.04 / −0.05	−0.00 / 0.00	0.01 / −0.01	0.06
	TiI	4.95	2.73	−2.22	0.17	19	0.02	0.03 / −0.05	0.00 / −0.01	0.01 / −0.01	0.05
	TiII	4.95	2.89	−2.06	0.28	6	0.04	0.04 / −0.04	0.02 / −0.02	−0.05 / 0.07	0.08
	CrI	5.64	3.03	−2.61	−0.22	4	0.02	0.01 / −0.02	−0.01 / 0.01	0.01 / −0.01	0.03
	NiI	6.22	3.85	−2.37	0.02	11	0.02	−0.04 / 0.05	0.02 / −0.02	0.04 / −0.05	0.07
	ZnI	4.56	2.67	−1.89	0.50	2	0.00	−0.13 / 0.17	0.09 / −0.09	0.01 / −0.01	0.17
	SrII	2.87	...	...	...	0	...	...	...	...	...
	BaII	2.18	−0.68	−2.86	−0.53	3	0.07	0.09 / −0.09	−0.01 / 0.01	−0.08 / 0.11	0.14